

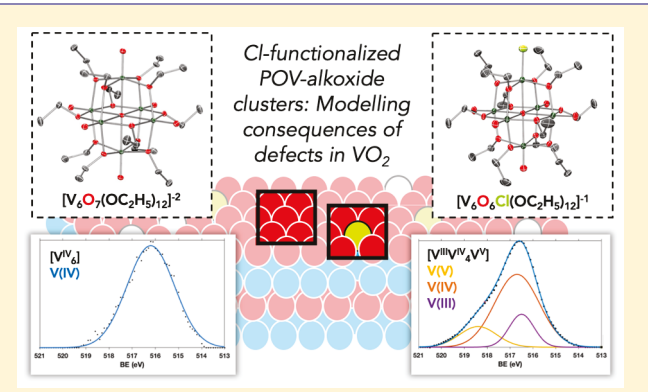
Site-Selective Halogenation of Polyoxovanadate Clusters: Atomically Precise Models for Electronic Effects of Anion Doping in VO₂

Brittney E. Petel, †,§ Rachel L. Meyer, †,§ Michela L. Maiola,† William W. Brennessel,† Astrid M. Müller,*^{,‡} and Ellen M. Matson*^{,†}

[†]Department of Chemistry and [‡]Department of Chemical Engineering, University of Rochester, Rochester, New York 14627, United States

Supporting Information

ABSTRACT: We report the synthesis and characterization of a monochloride-functionalized polyoxovanadate-alkoxide (POValkoxide) cluster, which can serve as a molecular model for halogen-doped vanadium oxide (VO2) materials that have recently attracted great interest as advanced materials for energy-saving smart window applications. Chloride-substituted variants of the Lindqvist vanadium-oxide cluster were obtained via two distinct chemical pathways: (1) direct halogenation of the isovalent parent POV-alkoxide architecture, $[V_6O_7(OC_2H_5)_{12}]^{-2}$ with AlCl₃ and (2) coordination of a chloride ion to a coordinatively unsaturated vanadium center within a cluster that bears a single oxygen-atom vacancy, $[V_6O_6(OC_2H_5)_{12}]^{12}$ Notably, our direct halogenation constitutes the first example of selective, single-site halide doping of homometallic metal oxide



clusters. The chloride-containing compound, $[V_6O_6Cl(OC_2H_5)_{12}]^{-1}$, was characterized by ¹H NMR spectroscopy and X-ray crystallography. The electronic structure of the chloride-functionalized POV-alkoxide cluster was established by infrared, electronic absorption, and X-ray photoelectron spectroscopy and revealed formation of a site-differentiated VIII ion upon halogenation. Cyclic voltammetry was employed to assess the electrochemical response of halide doping. A comparison of the Cl-VO_2 model to the fully oxygenated cluster, $[V_6O_7(OC_2H_5)_{12}]^{-2}$, provides molecular-level insights into a new proposed mechanism by which halogenation increases the carrier density in solid VO2, namely, through prompting charge separation within the material.

■ INTRODUCTION

Vanadium oxides have attracted great interest from the materials science and chemical engineering communities because of their rich electronic and physical properties. The wide range of oxidation states accessible to vanadium has resulted in the isolation of a variety of solid-state oxides (e.g., V₂O₅, VO₂, V₂O₃, VO, etc.), many of which exhibit intriguing optical, electrical, thermal, and magnetic properties.²⁻⁷ In particular, vanadium dioxide (VO₂) has benefitted from extensive research, given its near-room-temperature metal-toinsulator phase transition. This distinct property has resulted in the implementation of VO_2 films in energy-saving smart window technologies. $^{8-10}$

Recent developments aimed at the optimization of the photophysical and physicochemical properties of VO₂ (e.g., critical temperature, coloration) have revealed that atomic dopants serve to modulate the phase-transition mechanism and electronic structure of these materials. 11,12 In particular, anionic defects, in the form of halide ions, have been credited with substantially lowering the reversible metal-to-insulator transition temperature and band gap while maintaining the excellent visible transmittance and solar modulation of native VO_2 (Figure 1). Although theoretical studies have investigated the electronic structure of halide-doped VO₂ systems in the monoclinic phase, 18 challenges in isolating materials with the atomically precise and uniform incorporation of halide dopants have, to date, rendered a deep understanding of the electronic effects of said defects in VO2 unattainable.

Research targeting an improved understanding of the photophysical properties of first-row transition-metal oxides has revealed that the photoexcited states of these materials are best described by localized (cluster-like) electronic interactions. 19-21 These findings qualify metal oxide clusters as reasonable candidates for probing the electronic structure of corresponding solid oxide materials. Although no molecular model can fully capture the complex Mott physics and electron

Received: November 4, 2019 Published: December 18, 2019

Anionic Defects in Metal Oxides

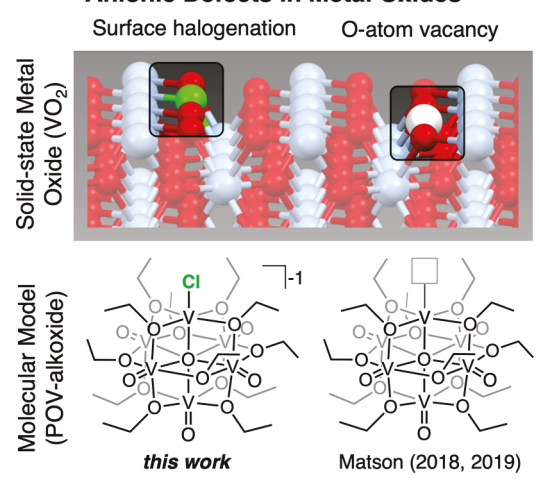


Figure 1. Schematic illustration of anionic defects in solid vanadium dioxide (top; structure for visualization only) and molecular POV-alkoxide clusters as models (bottom).^{33–35}

correlation effects observed for VO_2 because of the strong coupling among lattice, orbital, and spin degrees of freedom, such molecular systems are useful because they permit the use of spectroscopic techniques reserved for homogeneous (soluble) systems to gain structural, electronic, and mechanistic insights.

The Lindqvist architecture of polyoxovanadate-alkoxide (POV-alkoxide) clusters constitutes an excellent model system for solid VO₂ (Figure 1). ^{23–25} Although most commonly used polyoxovanadate clusters are composed of d^0 vanadium centers with four or five oxygen atoms oriented around the metal in a tetrahedral or square pyramidal geometry, the hexavanadate POV-alkoxide assembly prescribes an octahedral coordination environment for each vanadium center. ^{23,26} This immediate chemical environment of the six vanadium centers is rare for molecular vanadium oxide clusters and notably resembles that of individual vanadium ions found in VO₂. ²⁷ Likewise, the +4 oxidation state of all six vanadium ions in the dianionic (fully reduced) form of this cluster is electronically similar to the V^{IV} ions that comprise solid-state VO₂. Taken together, the physical and electronic properties of these POV-alkoxide clusters render them excellent molecular models for solid-state VO₂.

Although halide-templated vanadates exist, ^{28,29} they do not constitute good models for surface-halogenated VO₂. A majority of these systems possess vanadate ions that encapsulate halide ions, stitched together by electrostatic interactions. Here, we describe a POV-alkoxide cluster with a

coordinatively bound chloride ion at its surface, resulting in a spectroscopic model for surface-halogenated VO₂.

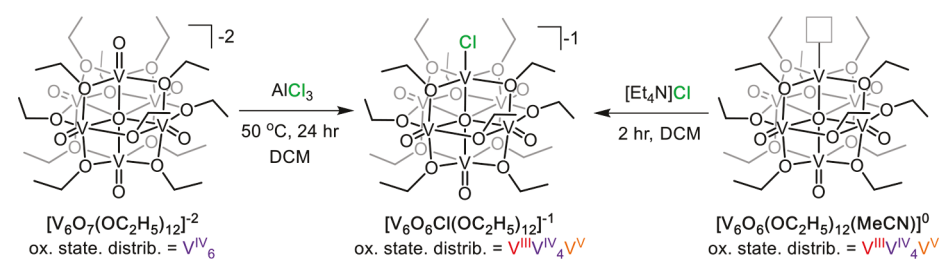
Previous work by our laboratory has focused on understanding synthesis routes for the formation of "doped" POV-alkoxide clusters. Our curiosity regarding the design of these types of molecular systems is based on their ability to serve as homogeneous and atomically precise models for extended solids. Early studies from our research group summarized results pertaining to the installation of high- (e.g., Ti^{IV})^{30,31} and low- (e.g., Fe^{III}, Ga^{III})^{32–34} valent cationic dopants within the Lindqvist framework via solvothermal synthesis. More recently, we have developed routes for the postsynthesis engineering of oxygen-atom defect sites at terminal oxido positions within these molecular metal oxide assemblies, presenting a rare example of an electronic and functional model of an anionic surface dopant.^{35–37}

Interested in expanding the scope of our work to other atomically precise, anionically doped VO2 architectures, we sought to develop synthesis routes to access halide-functionalized variants of the POV-alkoxide assembly. We opted to begin our studies with chloride ion installation because of results summarized in a recent theoretical study predicting that the incorporation of this halogen at the surface of VO2 would likely yield materials with optimal thermochromic performance for smart window applications (e.g., low critical temperature, small band gap). 18 Here, we report the site-selective chlorination of a reduced POV-alkoxide cluster. We view these halogenated clusters as model systems for Cl-doped VO₂, highlighting potential chemical routes for the controlled introduction of halide ions at the surface of this solid-state material. We subsequently present the spectroscopic characterization of the POV-alkoxide cluster bearing a site-differentiated "V-Cl" moiety. Comparison of the electronic structures of the fully oxygenated POV-alkoxide cluster and its halogenated congener offers insight into the localized electronic effects of halide doping in VO₂.

RESULTS AND DISCUSSION

Formation of $[V_6O_6Cl(OC_2H_5)_{12}]^-$: Direct Halogenation and Independent Synthesis. We chose to begin our investigations by developing synthesis pathways for the direct halogenation of the dianionic POV-alkoxide cluster, $[^nBu_4N]_2[V_6O_7(OC_2H_5)_{12}]$ (1- $V_6O_7^{-2}$). The molecular hexavanadate assembly is composed of six vanadium(IV) centers, 23 rendering its electronic structure most similar to that of VO_2 . The addition of 2 equiv of $AlCl_3$ to $1-V_6O_7^{-2}$ resulted in an immediate color change from blue-green to brown. Notably, the hue of the resulting compound is consistent with that observed for halide-doped VO_2 nanoparticles. 13 Analysis of the crude reaction mixture by 1H NMR

Scheme 1. Synthesis of $3\text{-V}_6\mathrm{O}_6\mathrm{Cl}^{-1}$ via Direct Halogenation of the Parent POV-Ethoxide Cluster $(1\text{-V}_6\mathrm{O}_7^{-2})$ and Surface Passivation of a POV-Ethoxide Cluster Bearing a Single Oxygen-Atom Defect $(2\text{-V}_6\mathrm{O}_6\mathrm{MeCN})$ with $[Et_4\mathrm{N}]\mathrm{Cl}$



spectroscopy revealed nearly complete conversion of the starting material (Scheme 1, Figure S1). The distribution of new, paramagnetically shifted and broadened resonances suggested a reduction in symmetry from that of the pseudo-octahedral parent cluster. This pattern of signals is consistent with the formation of the desired monohalogenated POV-alkoxide because the substitution of a single terminal oxido moiety by chloride would afford a Lindqvist cluster with pseudo- $C_{4\nu}$ symmetry.

Although ¹H NMR analysis showed that a new cluster was formed upon addition of AlCl₃ to $1-V_6O_7^{-2}$, electrochemical analysis by cyclic voltammetry revealed a complicated mixture of products (Figure S2). All attempts to purify the product of the reaction were thwarted because of similar solubilities of the presumed halogenated species and the starting material. Similar challenges in separating fully oxygenated and sitedifferentiated clusters have been noted previously by our laboratory. 32,34,36 Thus, we sought to independently synthesize a chlorinated variant of the homometallic POV-alkoxide assembly. Coordinatively unsaturated $[VO_x]^{-n}$ (x = 4, 5) fragments in polyoxovanadate architectures have been reported to bind electron-rich substrates (e.g., halide atoms, coordinating solvent molecules) at the unoccupied sites of the metal centers.²⁹ We therefore postulated that the installation of a halide at the surface of the POV-alkoxide assembly might be accomplished by the addition of a chloride-containing salt to a cluster featuring a coordinatively unsaturated vanadium ion.

To this end, we built upon the recently reported synthesis of a POV-ethoxide cluster with a single oxygen-atom vacancy ($[V_6O_6(OC_2H_5)_{12}(MeCN)]^0$; MeCN = acetonitrile, 2- V_6O_6MeCN). Upon addition of 1 equiv of tetraethylammonium chloride ($[Et_4N]Cl$) to complex 2- V_6O_6MeCN , we were able to access the chloride-functionalized variant of the cluster, $[Et_4N][V_6O_6Cl(OC_2H_5)_{12}]$ (3- $V_6O_6Cl^{-1}$, Scheme 1), as confirmed by electrospray ionization mass spectrometry (ESI-MS; Figure S3). Analysis of the product, 3- $V_6O_6Cl^{-1}$, by 1H NMR spectroscopy showed five paramagnetically shifted resonances located at 26.00, 24.45, -0.81, -2.17, and -22.54 ppm (Figure S4). A comparison of the 1H NMR spectra of 3- $V_6O_6Cl^{-1}$ with that of the product from the reaction of AlCl₃ and $1-V_6O_7^{-2}$ revealed virtually identical signals, suggesting that the same product is formed in both reactions.

Unambiguous assignment of the molecular structure of 3- $V_6O_6CI^{-1}$ was obtained via single-crystal X-ray diffraction (SCXRD). X-ray analysis of crystals that were grown by the vapor diffusion of pentane into a tetrahydrofuran solution of the product confirmed the connectivity and composition of the molecular structure of 3- $V_6O_6CI^{-1}$ (Figure 2, Table S1). Unfortunately, rigorous analysis of bond metrics of the Lindqvist assembly was not possible because of disorder within the unit cell. Regardless, these results, in summation, confirm that the product of the direct chlorination of the POV-ethoxide cluster was, in fact, the monohalogenated species.

Although halide-functionalized polyoxometalate clusters are highly relevant molecular models for solid-state, halide-doped transition-metal oxides, to the best of our knowledge there exist no examples that describe the electronic effects of the incorporation of these types of ligands at the surface of polyoxometalate assemblies. This is likely due to the fact that only a handful of reports exist that describe the synthesis of homometallic metal oxide clusters that contain surface halide ligands.^{38,39} The scarcity of polyoxometalate architectures that bear halide defect sites has been attributed to the instability of

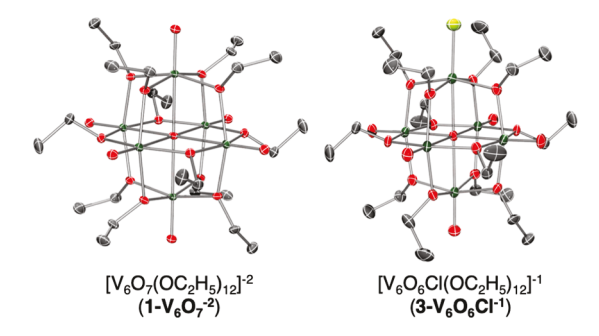


Figure 2. Molecular structures of $1\text{-V}_6O_7^{-2}$ and $3\text{-V}_6O_6\text{Cl}^{-1}$ shown with 50% probability ellipsoids. Hydrogen atoms, solvent molecules, and the counterion within the unit cell have been omitted for clarity. Crystallographic parameters for these structures are summarized in Tables S1 and S2. Colors: C, black; O, red; V, dark green; Cl, light green.

plenary structures (e.g., Keggin, Wells-Dawson polyoxoanions) in the presence of halogenating reagents. ^{39–41} Our synthesis approach of integrating a single chloride ion at the surface of a POV-alkoxide via postsynthetic functionalization constitutes a rare example of controlled, site-selective halogenation at the surface of a homometallic polyoxometalate cluster.

It is worth noting that while a dearth of polyoxometalate complexes exists with surface halide ligands, these ions are often incorporated at the center of metal oxide clusters. Indeed, halide and polyatomic anions have been reported as "templating" reagents for the synthesis of polyoxovanadate clusters. However, many of these previously reported vanadium oxide clusters do not constitute good models for Cl-doped VO₂ because they are composed of V^V centers (homo- and mixed-valent). Although some assemblies exist that are composed solely of V^{IV} moieties, weak electrostatic interactions to the interstitial halide ion render these systems suboptimal for modeling the electronic consequences of halide incorporation in VO₂.

Spectroscopic Analysis of a Cl-Doped POV-Alkoxide Cluster. With analytically pure samples of the halogenated product in hand, we turned our focus to the elucidation of the electronic structure of the chloride-functionalized Lindqvist assembly. Charge balancing suggests that the oxidation state distribution of vanadium moieties in complex 3-V₆O₆Cl⁻¹ could be assigned either as $\begin{bmatrix} V^{IV}_{6} \end{bmatrix}$ or as $\begin{bmatrix} V^{III}V^{IV}_{4}V^{V} \end{bmatrix}$. Previous reports by our laboratory 30,33,335-37,46 and others 24,25 have documented well-established spectroscopic features in the visible and near-infrared regions of the electronic absorption spectra of mixed-valent (VIV/V) POV-alkoxide clusters. Intervalence charge transfer (IVCT) bands were observed for POV-alkoxide clusters that possess VV centers, corresponding to the exchange of electron density between \dot{V}^{IV} and \dot{V}^{V} ions. Thus, we collected the electronic absorption spectrum of the halogenated cluster in acetonitrile (Figure 3) to distinguish between the two proposed oxidation-state distributions for complex $3-V_6O_6Cl^{-1}$.

Two distinct IVCT bands were observed at 398 nm ($\varepsilon = 3710~\text{M}^{-1}~\text{cm}^{-1}$) and 1000 nm ($\varepsilon = 478~\text{M}^{-1}~\text{cm}^{-1}$), consistent with the presence of a V^V center in the POV-alkoxide architecture (Figure 3). The higher-energy feature corresponds to a $d_{xy}(V^{IV}) \rightarrow d_{x2-y2}(V^{V})$ transition, while the lower energy is assigned to the $d_{xy}(V^{IV}) \rightarrow d_{xy}(V^{V})$ event. By comparison, the isovalent parent cluster, $1\text{-V}_{6}\text{O}_{7}^{-2}$, exhibits only a weak transition at 652 cm⁻¹ ($\varepsilon = 47~\text{M}^{-1}~\text{cm}^{-1}$), assigned to the

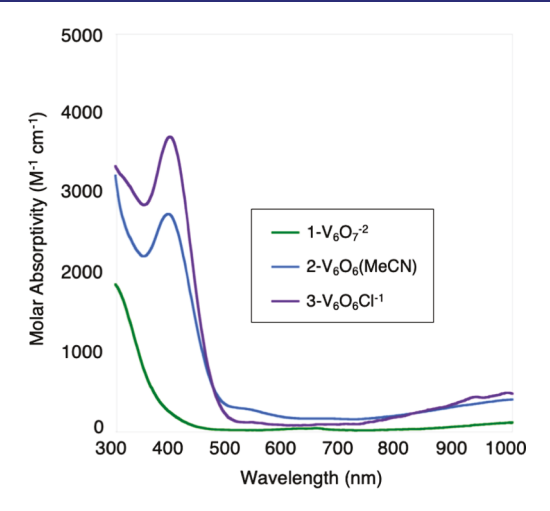


Figure 3. Electronic absorption spectra of $1\text{-}V_6O_7^{-2}$ (green), $2\text{-}V_6O_6MeCN$ (blue), and $3\text{-}V_6O_6Cl^{-1}$ (purple) collected in acetonitrile at $21\,^{\circ}C$.

excitation of a localized d electron at a d^1 vanadium center. 24,25 The presence of these absorbance features points toward a mixed-valent oxidation-state distribution of vanadium ions in complex $3\text{-V}_6\mathrm{O}_6\mathrm{Cl}^{-1}$, best described as $[V^{\mathrm{III}}V^{\mathrm{IV}}_{\phantom{\mathrm{A}}}V^{\mathrm{V}}]$. Further support for this assignment of the electronic structure of the halogenated POV-alkoxide cluster can be obtained from a comparison of the electronic absorption spectrum of $3\text{-V}_6\mathrm{O}_6\mathrm{Cl}^{-1}$ with that of complex $2\text{-V}_6\mathrm{O}_6\mathrm{MeCN}$. The oxygenatom-deficient POV-ethoxide cluster has been reported to have an analogous oxidation state distribution of vanadium ions, $[V^{\mathrm{III}}V^{\mathrm{IV}}_{\phantom{\mathrm{A}}}V^{\mathrm{V}}]$, to that proposed for $3\text{-V}_6\mathrm{O}_6\mathrm{Cl}^{-1}$. Indeed, the electronic absorption spectrum of complex $2\text{-V}_6\mathrm{O}_6\mathrm{MeCN}$ possesses two IVCT bands centered at 392 (ε = 2740 M⁻¹ cm⁻¹) and 1000 nm (ε = 407 M⁻¹ cm⁻¹).

Evidence for the change in the oxidation state distribution of vanadium ions within the cluster upon surface chlorination was obtained via X-ray photoelectron spectroscopy (XPS, Figure 4). This spectroscopic technique has been widely used to analyze the elemental composition or metal oxidation states in solid-state materials and also as a method for monitoring the reaction progress, effects of pretreatments, and aging of catalysts for both heterogeneous systems and molecular inorganic complexes.⁴⁷ The XPS data of $1-V_6O_7^{-2}$ exhibited a single peak in the energy region of V $2p_{3/2}$ at 516.2 eV, consistent with an isovalent $\left[V^{IV}_{6}\right]$ oxidation state distribution. In the case of 3-V₆O₆Cl⁻¹, the V 2p region showed two features for V $2p_{3/2}$ and V $2p_{1/2}$, ranging from \sim 513 to \sim 528 eV. Resolution of the vanadium energy region for V 2p_{3/2} revealed three vanadium peaks at 516.5, 516.7, and 518.4 eV, which can be attributed to vanadium ions in the 3+, 4+, and 5+ oxidation states, respectively. Integrated areas under curves from Gaussian fits at the aforementioned vanadium peak maxima were consistent with the proposed $[V^{III}V^{IV}_{4}V^{V}]$ oxidation state distribution (VIII 16.8%, VIV 67.3%, and VIII 15.8%). These data further validate the assignment of the electronic structure of the cluster inferred from electronic absorption spectroscopy. Thus, we can conclude that the chlorination of a single vanadyl site within the isovalent Lindqvist structure $(1 \cdot V_6 O_7^{-2})$ induces the disproportionation of two V^{IV} centers into a V^{III} and a V^{V} ion.

It is worth noting that in the single publication that describes the synthesis of Cl-doped VO_2 nanoparticles, XPS analysis

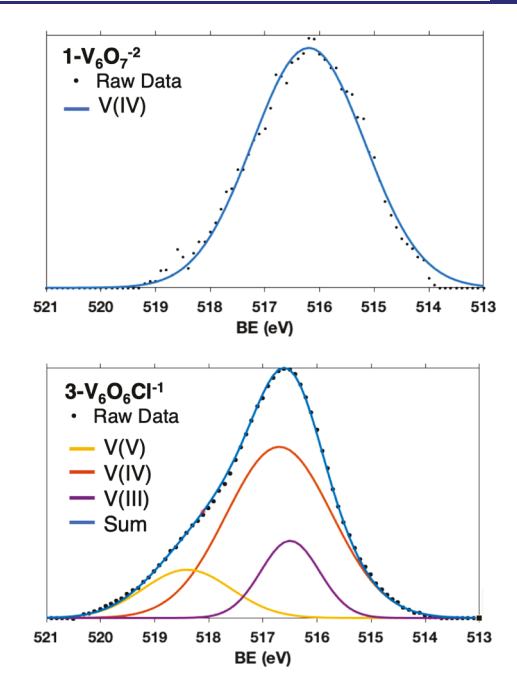


Figure 4. X-ray photoelectron spectra of the V 2p region of $1-V_6O_7^{2-}$ (top) and V $2p_{3/2}$ region of $3-V_6O_6CI^{-1}$ (bottom).

reveal the presence of both VIV and VV ions. 16 The authors attribute this observation to surface oxidation of the sample during analysis. However, our results offer an alternative explanation. Correlating the observation of V^V ions in the sample with our results obtained from XPS analysis of atomically precise models for Cl-doped VO2 implies that the disproportionation of vanadium ions across the material $(V^{IV}, \rightarrow V^{III}V^{V})$ would be required for the coordination of the chloride ligand at a site-differentiated VIII center. This, in turn, suggests that the V^V "impurity" observed in a previous analysis of Cl-doped materials might actually be a result of the substitution of an oxide ligand for a chloride ion at the surface of the nanoparticle. Indeed, a close examination of the XPS data for the model systems (V 2p region) reveals significant overlap in the features located in the V 2p region of XPS data corresponding to VIII and VIV ions. Thus, this analytical technique would be insufficient to make this electronic structure assignment in solid-state Cl-doped VO₂.

Overall, spectroscopic characterization of complex 3-V₆O₆Cl^{−1} deepens our understanding of the electronic effects of halogenation at VO₂ surfaces. Although halogen-free complex 1-V₆O₇⁻² possesses a symmetric Lindqvist core composed of six chemically equivalent V^{IV} ions, 24,25,48 the formation of one V-Cl bond results in site differentiation of a reduced VIII center. This, in turn, decouples the chlorinated vanadium ion from the vanadyl moieties that make up the rest of the POV-alkoxide cluster, allowing for the existence of both VIII and VV centers within a single metal oxide unit. This surprising change in the vanadium oxidation state distribution in the Lindqvist structure upon halogenation suggests that multiple mechanisms may contribute to the increased carrier density that has been theroetically predicted for halide-doped VO₂ (e.g., charge separation across the material).¹⁷ It remains unclear from our interpretation of preceding theoretical predictions, aimed at describing the electronic structure of these types of anionically doped materials, whether these changes in the oxidation states of individual vanadium centers

have been taken into consideration. Indeed, the clear disproportionation $(V^{IV}_2 \rightarrow V^{III}V^V)$ prompted by surface halogenation in our model systems suggests that changes in the oxidation states of vanadium ions might be important in the derivation of electronically precise density-of-state diagrams for halide-doped VO_2 materials.

Electrochemical Analysis: Elucidating the Electronic Effects of Surface Halogenation of VO₂. Further insight into the electronic effects of surface halogenation of the POV-ethoxide cluster was obtained via cyclic voltammetry (CV; Figure 5, Table 1). Lindqvist POV-alkoxide clusters possess

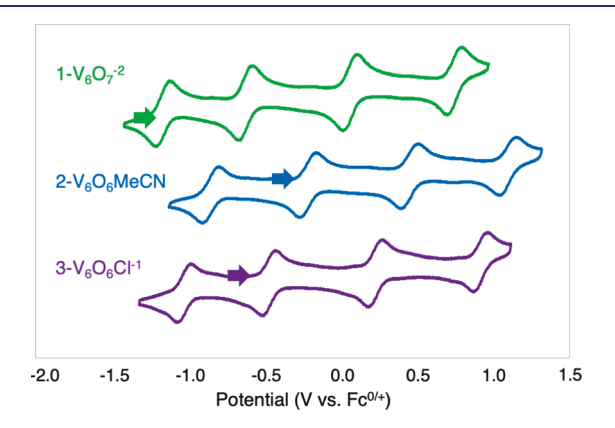


Figure 5. Cyclic voltammograms of complexes $1\text{-V}_6\mathrm{O}_7^{2-}$ (green), $2\text{-V}_6\mathrm{O}_6\mathrm{MeCN}$ (blue), and $3\text{-V}_6\mathrm{O}_6\mathrm{Cl}^{-1}$ (purple) collected in dichloromethane with 0.1 M [${}^n\mathrm{Bu}_4\mathrm{N}$][PF $_6$] as the supporting electrolyte.

rich electrochemical profiles, featuring up to four quasi-reversible redox events over a 1.7 V range. 24,25,46 Their electronic properties have been shown to be sensitive to the substitution of a transition metal or metalloid for a vanadyl moiety with the hexavanadate framework $^{30,32-34,49}$ and to be nominally unaffected by ligand substitution at the bridging-alkoxide sites. 50 Like its fully oxygenated congener, the CV of complex $\mathbf{3-V_6O_6Cl^{-1}}$ exhibited four quasi-reversible redox events ($E_{1/2}=+0.92, +0.23, -0.47, -1.02$ V vs $\mathbf{Fc^{0/+}}$ in dichloromethane). The anodic shift of the redox profile of the POV-ethoxide cluster upon halogenation (\sim 0.2 V) is consistent with the anticipated increase in the electron density thought to accompany the n-type doping of a solid metal oxide.

The implications of the shifts of the redox events of complex $3\text{-}V_6O_6\text{Cl}^{-1}$, in particular, how the change in energy of the electrochemical processes might provide information on anticipated changes in the band gap diagram for Cl-doped VO_2 , are worth considering. The four quasi-reversible electrochemical events observed in our CV data of $1\text{-}V_6O_7^{-2}$ and $3\text{-}V_6O_6\text{Cl}^{-1}$ correspond to vanadium-based oxidations $(V^{\text{IV}/\text{V}})$; as such, we can assign these events to the frontier orbitals that contribute to the valence band edge in the solid-state system. Theoretical investigations on the electronic

structure of solid-state VO_2 predict that the incorporation of halide dopants would result in the narrowing of the band gap of the material by increasing the energy of the valence band. However, the anodic shifts observed upon surface doping of the POV-alkoxide clusters are inconsistent with this proposed electronic structure, instead suggesting stabilization of the valence band upon incorporation of a surface chloride ion.

The inconsistencies noted in our electrochemical analysis of the POV-alkoxide clusters and theoretical band diagrams predicted for Cl-doped VO₂ might be attributed to the fact that these model systems are molecular species. Inherently, these clusters do not take into consideration the complicated electronic structures and Mott physics of extended vanadates. However, the color of the POV-alkoxide upon surface halogenation is consistent with that reported for the monoclinic phase of Cl-doped VO₂ (yellow/brown), suggesting that the predicted shifts in the valence band edge of Cl-doped VO₂ are not solely responsible for the changes in the optical behavior of this material. Instead, our molecular models posit that the change in color of Cl-doped VO₂ is likely due to the formation of midgap states that give rise to new, lower-energy visible absorption processes for this material.

Our synthetic handle on atomically precise vanadium oxide assemblies that bear surface defects allows for the comparison of the electronic consequences of disparate anionic dopants. We can therefore compare the CV of complex $3-V_6O_6Cl^{-1}$ to that of a POV-alkoxide bearing a single oxygen atom vacancy (2-V₆O₆MeCN). This analysis provides insight into the differences in the localized electronic structures of metal oxide materials with varying types of anionic defect sites (i.e., oxygen-atom vacancy vs chloride dopant). The $E_{1/2}$ values of all four electrochemical events were shifted cathodically from that of complex 2-V₆O₆MeCN ($E_{1/2} = +1.11, +0.46, -0.21,$ -0.85 V vs Fc^{0/+} in dichloromethane, Figure 5, Table 1).³⁷ We attribute these shifts to the change in overall charge of the halogenated species; the POV-ethoxide cluster takes on a negative charge upon coordination of the chloride atom to the surface defect site. However, we cannot rule out the π -donating character of the chloride ligand in complex 3-V₆O₆Cl⁻¹ as a contributing factor in the observed shifts in redox potentials of the cluster. In either case, the cathodic shifts of all four redox events indicate that surface passivation of oxygen-atom vacancies with chloride ions results in a vanadium oxide assembly that possesses a higher activation energy for the introduction of excess electron density to the cluster core.

CONCLUSIONS

We have established a synthesis route for the direct, site-selective monohalogenation of metal oxide clusters via addition of AlCl₃ to an isovalent POV-alkoxide cluster, $1-V_6O_7^{-2}$. Independent preparation of $3-V_6O_6CI^{-1}$ by the addition of $[Et_4N]Cl$ to a POV-ethoxide cluster with a single O atom vacancy confirmed the atomically precise installation of a single

Table 1. Electrochemical Parameters of Complexes 1-V₆O₇⁻², 2-V₆O₆MeCN, and 3-V₆O₆Cl⁻¹

redox couple of $1-V_6O_7^{-2}$	$E_{1/2}(V)^a$	redox couple of 2-V ₆ O ₆ MeCN	$E_{1/2}(V)^a$	redox couple of $3-V_6O_6Cl^{-1}$	$E_{1/2}(V)^a$
$[{\rm V^{IV}}_6]/[{\rm V^{IV}}_5{\rm V^V}]$	-1.16	$[V^{III}V^{IV}_{5}]/[V^{III}V^{IV}_{4}V^{V}]$	-0.85	$[V^{III}V^{IV}_{5}]/[V^{III}V^{IV}_{4}V^{V}]$	-1.02
$[V^{IV}_{5}V^V]/[V^{IV}_{4}V^V_{2}]$	-0.62	$\big[V^{III}V^{IV}_{4}V^V\big]/\big[V^{III}V^{IV}_{3}V^V_{2}\big]$	-0.21	$\left[V^{III}V^{IV}_{4}V^{V}\right]/\left[V^{III}V^{IV}_{3}V^{V}_{2}\right]$	-0.47
$[V_{4}^{IV}V_{2}^{V}]/[V_{3}^{IV}V_{3}^{V}]$	+0.07	$\big[\boldsymbol{V^{III}}\boldsymbol{V^{IV}}_{3}\boldsymbol{V^{V}}_{2}\big]/\big[\boldsymbol{V^{III}}\boldsymbol{V^{IV}}_{2}\boldsymbol{V^{V}}_{3}\big]$	+0.46	$\big[\boldsymbol{V^{III}}\boldsymbol{V^{IV}}_3\boldsymbol{V^{V}}_2\big]/\big[\boldsymbol{V^{III}}\boldsymbol{V^{IV}}_2\boldsymbol{V^{V}}_3\big]$	+0.23
$[V_{3}^{IV}V_{3}^{V}]/[V_{2}^{IV}V_{4}^{V}]$	+0.75	$[{\rm V^{III}V^{IV}}_2{\rm V^V}_3]/[{\rm V^{III}V^{IV}V^V}_4]$	+1.11	$[{\mathbf{V}^{\mathrm{III}}}{\mathbf{V}^{\mathrm{IV}}}_{2}{\mathbf{V}^{\mathrm{V}}}_{3}]/[{\mathbf{V}^{\mathrm{III}}}{\mathbf{V}^{\mathrm{IV}}}{\mathbf{V}^{\mathrm{V}}}_{4}]$	+0.92

^aAll $E_{1/2}$ values are reported on the basis of data collected in dichloromethane and referenced vs Fc^{0/+}.

surface-bound chloride ligand at the metal oxide assembly. Structural and spectroscopic characterization by X-ray crystallography and electronic absorption, infrared, and X-ray photoelectron spectroscopy revealed a mixed-valent oxidation state distribution $[V^{III}V^{IV}_{4}V^{V}]$ in the halogenated compound. Importantly, these results present two distinct chemical pathways for the postsynthetic formation of model Cl-doped VO₂ complexes, with implications for the development of superior smart window technologies.

The isolation of complex $3-V_6O_6Cl^{-1}$ has provided us with opportunities to probe the localized electronic effects of surface halogenation. Indeed, comparing the halogenated cluster to its fully oxygenated congeners via electroanalysis revealed that surface halogenation results in an anodic shift in redox potentials. Overall, our results demonstrate how controlled surface halogenation affects the localized electronic structure in vanadium oxide moieties, with direct ramifications on understanding anion doping in vanadium dioxide smartwindow materials toward optimized energy-saving performance.

EXPERIMENTAL SECTION

General Considerations. All manipulations, unless otherwise noted, were carried out in the absence of water and oxygen in a UniLab MBraun inert atmosphere glovebox under a dinitrogen atmosphere. Glassware was oven-dried for a minimum of 4 h and cooled in an evacuated antechamber prior to use in the drybox. Unless otherwise noted, solvents were dried and deoxygenated on a Glass Contour System (Pure Process Technology, LLC) and stored over activated 3 Å molecular sieves purchased from Fisher Scientific. $["Bu_4N]_2[V_6O_7(OC_2H_5)_{12}]^{23}$ $(1-V_6O_7^{-2})$ and $[V_6O_6(OC_2H_5)_{12}MeCN]^{37}$ (2- V_6O_6MeCN) were prepared as previously reported. AlCl3 was purchased from Sigma-Aldrich and used

¹H NMR spectra were recorded at 400 MHz on Bruker DPX-400 MHz spectrometers locked on the signal of deuterated solvents. All chemical shifts were reported relative to the peak of the residual ¹H signal in deuterated solvents. CDCl₃ was purchased from Cambridge Isotope Laboratories, degassed by three freeze-pump-thaw cycles, and stored over activated 3 Å molecular sieves. Infrared (FT-IR, ATR) spectra of complexes were recorded on a Shimadzu IRAffinity-1 Fourier transform infrared spectrophotometer and are reported in wavenumbers (cm⁻¹). Electronic absorption measurements were recorded at room temperature in anhydrous acetonitrile in a sealed 1 cm quartz cuvette with an Agilent Cary 60 UV-vis spectrophotometer. Mass spectrometry analyses were performed on an Advion Expression^L compact mass spectrometer equipped with an electrospray probe and an ion-trap mass analyzer. Direct injection analysis was employed in all cases with a sample solution in acetonitrile. Single crystals were mounted on the tip of a thin glass optical fiber (goniometer head) and mounted on a Bruker SMART APEX II CCD platform diffractometer for data collection at 100.0(5) K. The structures were solved using SHELXT-2014/5⁵¹ and refined using SHELXL-2014/7.52 Elemental analyses were performed on a PerkinElmer 2400 Series II Analyzer at the CENTC Elemental Analysis Facility, University of Rochester.

Concentrations of active species for electrochemical analysis (vanadium oxide cluster) and [nBu4N][PF6] used were 1 and 100 mM, respectively, in dichloromethane. Prior to running electrochemical experiments, the supporting electrolyte was recrystallized three times from ethanol and stored under constant vacuum. CV measurements were carried out using a Bio-Logic SP 150 potentiostat/galvanostat and the EC-Lab software suite. Glassy carbon disks (3 mm, CH Instruments, USA) were used as working electrodes. Working electrodes were polished using a microcloth pad and 0.05 μ M alumina powder. Potentials recorded during CV were measured relative to a nonaqueous Ag/Ag+ reference electrode with

10 mM AgNO₃ and 100 mM [ⁿBu₄N][PF₆] in acetonitrile (Bio-Logic). A platinum wire served as the counter electrode. All experiments were carried out at room temperature inside a nitrogen-filled glovebox (MBraun, USA). All CV measurements were IR compensated at 85% with impedance taken at 100 kHz using the ZIR tool included with the EC-Lab software. All redox events were referenced against a ferrocenium/ferrocene (Fc+/Fc) redox couple.

X-ray photoelectron spectra (XPS) were taken using a Kratos Axis Ultra DLD. XPS sample preparation for 1-V₆O₇⁻² and 3-V₆O₆Cl⁻¹ was performed under a dinitrogen atmosphere in the glovebox. Samples were prepared by drop-casting solutions of concentrated samples in dry dichloromethane on cleaned Si wafers, which were grounded to the sample bar by carbon tape. Neutralizer settings: (current) 7×10^{-6} A; (charge balance) 5 eV; (filament bias) 1.3 V; (X-ray gun settings) 10 mA emission and 15 kV high tension (Al anode); and (collection settings) 80 eV pass energy for survey and region scans, three scans for vanadium, and two scans for nonmetals. Survey scans from 0 to 1200 eV were carried out to identify the elements present in the sample. Binding energies were referenced to the C 1s peak arising from adventitious carbon, taken to have a binding energy of 284.8 eV. 53,54 High-resolution spectra were collected for the V 2p, Cl 2p, C 1s, and O 1s regions. The V 2p region was increased to 510-540 eV to fit the V 2p and O 1s regions together. Quantitative peak areas were derived after Touggard background subtraction. Binding energies were obtained from the same peak fits. Quantitative XPS analysis was performed with CasaXPS (version 2.3.1).

Synthesis of $[^{n}Bu_{4}N]_{2}[V_{6}O_{7}(OC_{2}H_{5})_{12}]$ (1- $V_{6}O_{7}^{-2}$). The synthesis of $1-V_6O_7^{-2}$ was adapted from a previous report.⁴⁶ In a glovebox, a 15 mL pressure vessel was charged with $[V_6O_7(OC_2H_5)_{12}]^0$ (0.113 g, 0.0118 mmol) and approximately 10 mL of acetonitrile. Tetrabutylammonium hydroxide in methanol (0.35 mL, 0.35 mmol, 3 equiv) was added to the solution. The pressure vessel was removed from the glovebox and stirred at 90 °C for 24 h. The resulting solution was pumped back into the glovebox, filtered, and concentrated. The solution was stored at -35 °C for crystallization, affording blue crystals of complex $1\text{-}V_6{O_7}^{-2}.$ These crystals were suitable for X-ray analysis. Analytical data obtained for complex 1-V₆O₇⁻² via standard characterization techniques (¹H NMR, IR, and UV-vis) matched that obtained from the previously reported synthesis.⁴⁶

Synthesis of $[Et_4N][V_6O_6CI(OC_2H_5)_{12}]$ (3- $V_6O_6CI^{-1}$). A 20 mL scintillation vial was charged with 2-V₆O₆MeCN (0.060 g, 0.061 mmol) and approximately 6 mL of dichloromethane. Solid tetraethylammonium chloride (0.012 g, 0.075 mmol, 1.2 equiv) was added to the solution, and the reaction mixture was stirred at room temperature for 2 h. The volatiles were removed under reduced pressure. The resulting brown solid was crystallized from the diffusion of pentane into a concentrated tetrahydrofuran solution at room temperature, affording complex 3-V₆O₆Cl⁻¹ in good yield (0.047 g, 0.042 mmol, 69%). These crystals were suitable for X-ray analysis. ¹H NMR (400 MHz, CDCl₃): δ = 26.00 (fwhh = 430 Hz), 24.45 (fwhh = 360 Hz), -0.81 (fwhh = 190 Hz), -2.17 (fwhh = 210 Hz), -22.54(fwhh = 580 Hz) ppm. FT-IR (ATR, cm⁻¹): 1040 (O_b - C_2 H₅), 956 (V = O_t). UV-vis (CH₂Cl₂): 398 nm, (ε = 4495 M⁻¹ cm⁻¹), 1000 nm (ε = 590 M^{-1} cm⁻¹). Elemental analysis for $C_{32}H_{80}O_{18}V_6ClN$ (MW = 1107.64 g/mol) Calcd (%): C, 34.67; H, 7.28; N, 1.26. Found (%): C, 34.63; H, 7.36; N, 1.16.

Synthesis of [nBu4N][V6O6Cl(OC2H5)12] via Chlorination of $[V_6O_7(OC_2H_5)_{12}]^{2-}$ with AlCl₃. A 20 mL scintillation vial was charged with $1-V_6O_7^{-2}$ (0.030 g, 0.025 mmol) and approximately 6 mL of dichloromethane. Solid aluminum trichloride (0.008 g, 0.056 mmol, 2.2 equiv) was added to the solution, and the reaction mixture was stirred at 50 °C for 24 h. The volatiles were removed under reduced pressure to yield a brown solid. The residue was stirred in diethyl ether for 10 min and then filtered. The solid was continuously washed with diethyl ether until the filtrate was colorless. The solid was extracted with dichloromethane, and volatiles were removed under reduced pressure. The product was further purified via recrystallization from the slow diffusion of pentane into a concentrated solution of $3\text{-V}_6\mathrm{O}_6\mathrm{Cl}^{-1}$ in dichloromethane (0.023 g. 0.019 mmol, 75%). $^1\mathrm{H}$ NMR spectroscopy revealed a spectrum of the product that matched that of independently synthesized $3\text{-V}_6\mathrm{O}_6\mathrm{Cl}^{-1}$.

ASSOCIATED CONTENT

Supporting Information

The Supporting Information is available free of charge at https://pubs.acs.org/doi/10.1021/jacs.9b11874.

 ^{1}H NMR spectra of $1\text{-}V_{6}O_{7}^{-2}$, , $2\text{-}V_{6}O_{6}MeCN$, and $3\text{-}V_{6}O_{6}Cl^{-1}$; cyclic voltammogram of the crude mixture from the reaction of $1\text{-}V_{6}O_{7}^{-2}$ and AlCl₃; ESI-MS (-)ve of $3\text{-}V_{6}O_{6}Cl^{-1}$; and crystallographic parameters of $3\text{-}V_{6}O_{6}Cl^{-1}$ and $1\text{-}V_{6}O_{7}^{-2}$ (PDF)

Crystallographic Information File for complex 3-V6O6Cl-1 (MATRM17) (CIF)

Crystallographic Information File for complex 1-V6O7-2 (MATBP42) (CIF)

AUTHOR INFORMATION

Corresponding Authors

*astrid.mueller@rochester.edu

*matson@chem.rochester.edu

ORCID ®

William W. Brennessel: 0000-0001-5461-1825

Astrid M. Müller: 0000-0002-2785-6808 Ellen M. Matson: 0000-0003-3753-8288

Author Contributions

§These authors contributed equally.

Notes

The authors declare no competing financial interest.

ACKNOWLEDGMENTS

This research was funded by the National Science Foundation through grants CHE-1653195 and CHE-1725028 (B.E.P., R.L.M., M.L.M., and E.M.M.). The authors also acknowledge generous financial support from the University of Rochester through start-up funds. The authors thank Kathryn E. Knowles and David Brewster for helpful discussions and acknowledge the UR Nano facilities for technical support of the X-ray photoelectron spectrometer.

REFERENCES

- (1) Weckhuysen, B. M.; Keller, D. E. Chemistry, spectroscopy and the role of supported vanadium oxides in heterogeneous catalysis. *Catal. Today* **2003**, *78*, 25–46.
- (2) Livage, J. Optical and electrical properties of vanadium oxides synthesized from alkoxides. *Coord. Chem. Rev.* **1999**, 190–192, 391–403.
- (3) Wu, Q.-H.; Thissen, A.; Jaegermann, W.; Liu, M. Photoelectron spectroscopy study of oxygen vacancy on vanadium oxides surface. *Appl. Surf. Sci.* **2004**, *236*, 473–478.
- (4) Gossard, A. C.; Di Salvo, F. J.; Erich, L. C.; Remeika, J. P.; Yasuoka, H.; Kosuge, K.; Kachi, S. Microscopic magnetic properties of vanadium oxides. II. V₃O₅, V₆O₉, V₆O₁₁, and V₆O₁₃. *Phys. Rev. B* **1974**, *10*, 4178–4183.
- (5) Schwingenschlögl, U.; Eyert, V. The vanadium Magnéli phases $V^nO_2^{n-1}$. Ann. Phys. **2004**, 13 (9), 475–510.
- (6) Berglund, C. N.; Guggenheim, H. J. Electronic Properties of VO, near the Semiconductor-Metal Transition. *Phys. Rev.* **1969**, *185*, 1022–1033.
- (7) Wang, X.; Lin, Y.-C.; Zhou, H.; Omenya, F.; Chu, I.-H.; Karki, K.; Sallis, S.; Rana, J.; Piper, L. F. J.; Chernova, N. A.; Ong, S. P.;

- Whittingham, M. S. Structural Changes in a High-Energy Density VO₂F Cathode upon Heating and Li Cycling. *ACS Appl. Energy Mater.* **2018**, *1*, 4514–4521.
- (8) Xu, F.; Cao, X.; Luo, H.; Jin, P. Recent advances in VO2-based thermochromic composites for smart windows. *J. Mater. Chem. C* **2018**, *6*, 1903–1919.
- (9) Wu, C.; Wei, H.; Ning, B.; Xie, Y. New Vanadium Oxide Nanostructures: Controlled Synthesis and Their Smart Electrical Switching Properties. *Adv. Mater.* **2010**, 22, 1972–1976.
- (10) Cui, Y.; Ke, Y.; Liu, C.; Chen, Z.; Wang, N.; Zhang, L.; Zhou, Y.; Wang, S.; Gao, Y.; Long, Y. Thermochromic VO2 for Energy-Efficient Smart Windows. *Joule* 2018, 2, 1707–1746.
- (11) Wang, S.; Liu, M.; Kong, L.; Long, Y.; Jiang, X.; Yu, A. Recent progress in VO2 smart coatings: Strategies to improve the thermochromic properties. *Prog. Mater. Sci.* **2016**, *81*, 1–54.
- (12) Liu, Y.; Wang, W.; Xu, X.; Marcel Veder, J.-P.; Shao, Z. Recent advances in anion-doped metal oxides for catalytic applications. *J. Mater. Chem. A* **2019**, *7*, 7280–7300.
- (13) Dai, L.; Chen, S.; Liu, J.; Gao, Y.; Zhou, J.; Chen, Z.; Cao, C.; Luo, H.; Kanehira, M. F-doped VO₂ nanoparticles for thermochromic energy-saving foils with modified color and enhanced solar-heat shielding ability. *Phys. Chem. Chem. Phys.* **2013**, *15*, 11723–11729.
- (14) Burkhardt, W.; Christmann, T.; Franke, S.; Kriegseis, W.; Meister, D.; Meyer, B. K.; Niessner, W.; Schalch, D.; Scharmann, A. Tungsten and fluorine co-doping of VO₂ films. *Thin Solid Films* **2002**, 402, 226–231.
- (15) Khan, K. A.; Niklasson, G. A.; Granqvist, C. G. Optical properties at the metal-insulator transition in thermochromic $VO_{2-x}F_x$ thin films. *J. Appl. Phys.* **1988**, *64*, 3327–3329.
- (16) Riapanitra, A.; Asakura, Y.; Yin, S. One-step hydrothermal synthesis and thermochromic properties of chlorine-doped VO₂(M) for smart window application. *Funct. Mater. Lett.* **2019**, 1951008.
- (17) Bayard, M. L. F.; Reynolds, T. G.; Vlasse, M.; McKinzie, H. L.; Arnott, R. J.; Wold, A. Preparation and properties of the oxyfluoride systems $V_2O_{5-x}F_x$ and $VO_{2-x}F_x$. *J. Solid State Chem.* 1971, 3, 484–489. (18) Ren, Q.; Wan, J.; Gao, Y. Theoretical Study of Electronic Properties of X-Doped (X = F. Cl. Br. J.) VO. Nanoparticles for
- Properties of X-Doped (X = F, Cl, Br, I) VO₂ Nanoparticles for Thermochromic Energy-Saving Foils. *J. Phys. Chem. A* **2014**, 118, 11114–11118.
- (19) Biswas, S.; Husek, J.; Londo, S.; Baker, L. R. Highly Localized Charge Transfer Excitons in Metal Oxide Semiconductors. *Nano Lett.* **2018**, *18*, 1228–1233.
- (20) Biswas, S.; Husek, J.; Baker, L. R. Elucidating ultrafast electron dynamics at surfaces using extreme ultraviolet (XUV) reflection—absorption spectroscopy. *Chem. Commun.* **2018**, *54*, 4216–4230.
- (21) Biswas, S.; Husek, J.; Londo, S.; Fugate, E. A.; Baker, L. R. Identifying the acceptor state in NiO hole collection layers: direct observation of exciton dissociation and interfacial hole transfer across a Fe2O3/NiO heterojunction. *Phys. Chem. Chem. Phys.* **2018**, 20, 24545–24552.
- (22) Ishige, Y.; Sudayama, T.; Wakisaka, Y.; Mizokawa, T.; Wadati, H.; Sawatzky, G. A.; Regier, T. Z.; Isobe, M.; Ueda, Y. Interplay between Mott physics and Peierls physics in hollandite-type vanadates with a metal-insulator transition. *Phys. Rev. B: Condens. Matter Mater. Phys.* **2011**, 83, 125112.
- (23) Spandl, J.; Daniel, C.; Brüdgam, I.; Hartl, H. Synthesis and Structural Characterization of Redox-Active Dodecamethoxoheptaoxohexavanadium Clusters. *Angew. Chem., Int. Ed.* **2003**, 42, 1163–1166.
- (24) Daniel, C.; Hartl, H. Neutral and Cationic V^{IV}/V^V Mixed-Valence Alkoxo-polyoxovanadium Clusters $[V_6O_7(OR)_{12}]^{n+}$ (R = -CH₃, -C₂H₅): Structural, Cyclovoltammetric and IR-Spectroscopic Investigations on Mixed Valency in a Hexanuclear Core. *J. Am. Chem. Soc.* **2005**, *127*, 13978–13987.
- (25) Daniel, C.; Hartl, H. A Mixed-Valence V^{IV}/V^V Alkoxopolyoxovanadium Cluster Series $[V_6O_8(OCH_3)_{11}]^{n\pm}$: Exploring the Influence of a μ -Oxo Ligand in a Spin Frustrated Structure. *J. Am. Chem. Soc.* **2009**, *131*, 5101–5114.

- (26) Zhang, Y.-T.; Wang, X.-L.; Zhou, E.-L.; Wu, X.-S.; Song, B.-Q.; Shao, K.-Z.; Su, Z.-M. Polyoxovanadate-based organic—inorganic hybrids: from $\{V_sO_9Cl\}$ clusters to nanosized octahedral cages. *Dalton Trans.* **2016**, *45*, 3698–3701.
- (27) Oka, Y.; Sato, S.; Yao, T.; Yamamoto, N. Crystal Structures and Transition Mechanism of VO₂(A). *J. Solid State Chem.* **1998**, *141*, 594–598.
- (28) Healy, C.; Schmitt, W. Multicomponent halide templating: The effect of structure-directing agents on the assembly of molecular and extended coordination compounds. *Coord. Chem. Rev.* **2018**, *371*, 67–85.
- (29) Streb, C. Structure and Bonding in Molecular Vanadium Oxides: From Templates via Host—Guest Chemistry to Applications. In *Polyoxometalate-Based Assemblies and Functional Materials*; Song, Y.-F., Ed.; Springer International Publishing: Cham, 2018; pp 31–47.
- (30) VanGelder, L. E.; Brennessel, W. W.; Matson, E. M. Tuning the redox profiles of polyoxovanadate-alkoxide clusters via heterometal installation: toward designer redox Reagents. *Dalton Trans.* **2018**, 47, 3698–3704.
- (31) VanGelder, L. E.; Forrestel, P. L.; Brennessel, W. W.; Matson, E. M. Site-selectivity in the halogenation of titanium-functionalized polyoxovanadate—alkoxide clusters. *Chem. Commun.* **2018**, *54*, 6839—6842.
- (32) Meyer, R. L.; Brennessel, W. W.; Matson, E. M. Synthesis of a gallium-functionalized polyoxovanadate-alkoxide cluster: Toward a general route for heterometal installation. *Polyhedron* **2018**, *156*, 303–311.
- (33) Li, F.; Carpenter, S. H.; Higgins, R. F.; Hitt, M. G.; Brennessel, W. W.; Ferrier, M. G.; Cary, S. K.; Lezama-Pacheco, J. S.; Wright, J. T.; Stein, B. W.; Shores, M. P.; Neidig, M. L.; Kozimor, S. A.; Matson, E. M. Polyoxovanadate—Alkoxide Clusters as a Redox Reservoir for Iron. *Inorg. Chem.* **2017**, *56*, 7065—7080.
- (34) Li, F.; VanGelder, L. E.; Brennessel, W. W.; Matson, E. M. Self-Assembled, Iron-Functionalized Polyoxovanadate Alkoxide Clusters. *Inorg. Chem.* **2016**, *55*, 7332–7334.
- (35) Petel, B. E.; Brennessel, W. W.; Matson, E. M. Oxygen-Atom Vacancy Formation at Polyoxovanadate Clusters: Homogeneous Models for Reducible Metal Oxides. *J. Am. Chem. Soc.* **2018**, *140*, 8424—8428
- (36) Petel, B. E.; Fertig, A. A.; Maiola, M. L.; Brennessel, W. W.; Matson, E. M. Controlling Metal-to-Oxygen Ratios via M-O Bond Cleavage in Polyoxovanadate Alkoxide Clusters. *Inorg. Chem.* **2019**, 58, 10462–10471.
- (37) Petel, B. E.; Meyer, R. L.; Brennessel, W. W.; Matson, E. M. Oxygen atom transfer with organofunctionalized polyoxovanadium clusters: O-atom vacancy formation with tertiary phosphanes and deoxygenation of styrene oxide. *Chem. Sci.* **2019**, *10*, 8035–8045.
- (38) Streb, C. Structure and Bonding in Molecular Vanadium Oxides: From Templates via Host—Guest Chemistry to Applications. In *Polyoxometalate-Based Assemblies and Functional Materials*; Song, Y.-F., Ed.; Springer International Publishing: Cham, 2018; pp 31–47.
- (39) VanGelder, L. E.; Petel, B. E.; Nachtigall, O.; Martinez, G.; Brennessel, W. W.; Matson, E. M. Organic Functionalization of Polyoxovanadate—Alkoxide Clusters: Improving the Solubility of Multimetallic Charge Carriers for Nonaqueous Redox Flow Batteries. *ChemSusChem* 2018, 11, 4139—4149.
- (40) Kang, H.; Liu, S.; Shaikh, S. N.; Nicholson, T.; Zubieta, J. Synthesis and structural investigation of polyoxomolybdate coordination compounds displaying a tetranuclear core. Crystal and molecular structures of $[Bu_4N]_2[Mo_4O_{10}(OMe)_2(OC_6H_4O)_2]$ and to the d i a z e n i d o c o m p l e x e s $[Bu_4N]_2[Mo_4O_6(OMe)_2(HNC_6H_4O)_2(NNC_6H_5)_4]$ and $[Bu_4N]_2[Mo_4O_6(OMe)_2(C_{10}H_6O_2)_2(NNC_6H_5)_4]$. Comparison to a binuclear complex with the $[Mo_2(OMe)_2(NNC_6H_5)_4]^{2+}$ core, $[Mo_2(OMe)_2(H_2NC_6H_4O)]$. Inorg. Chem. 1989, 28, 920–933.
- (41) Errington, R. J.; Wingad, R. L.; Clegg, W.; Elsegood, M. R. J. Direct Bromination of Keggin Fragments To Give [PW₉O₂₈Br₆]³⁻: A Polyoxotungstate with a Hexabrominated Face. *Angew. Chem., Int. Ed.* **2000**, *39*, 3884–3886.

- (42) Knoth, W. H.; Domaille, P. J.; Roe, D. C. Halometal derivatives of $W_{12}PO_{40}^{3-}$ and related tungsten-183 NMR studies. *Inorg. Chem.* **1983**, 22, 198–201.
- (43) Lu, Y.-J.; Beer, R. H. The reaction of polynuclear tungstates with thionyl chloride: Formation of $(^nBu_4N)[W(O)Cl_5]$. Polyhedron 1996, 15, 1667–1671.
- (44) Kastner, K.; Margraf, J. T.; Clark, T.; Streb, C. A Molecular Placeholder Strategy To Access a Family of Transition-Metal-Functionalized Vanadium Oxide Clusters. *Chem. Eur. J.* **2014**, *20*, 12269–12273.
- (45) Zhang, C.-D.; Liu, S.-X.; Gao, B.; Sun, C.-Y.; Xie, L.-H.; Yu, M.; Peng, J. Hybrid materials based on metal—organic coordination complexes and cage-like polyoxovanadate clusters: Synthesis, characterization and magnetic properties. *Polyhedron* **2007**, *26*, 1514—1522.
- (46) Chen, L.; Jiang, F.; Lin, Z.; Zhou, Y.; Yue, C.; Hong, M. A Basket Tetradecavanadate Cluster with Blue Luminescence. *J. Am. Chem. Soc.* **2005**, *127*, 8588–8589.
- (47) Müller, A.; Krickemeyer, E.; Penk, M.; Walberg, H.-J.; Bögge, H. Spherical Mixed-Valence [V15O36]⁵⁻, an Example from an Unusual Cluster Family. *Angew. Chem., Int. Ed. Engl.* **1987**, 26, 1045–1046.
- (48) VanGelder, L. E.; Kosswattaarachchi, A. M.; Forrestel, P. L.; Cook, T. R.; Matson, E. M. Polyoxovanadate-alkoxide clusters as multi-electron charge carriers for symmetric non-aqueous redox flow batteries. *Chem. Sci.* **2018**, *9*, 1692–1699.
- (49) Furlani, C. XPS of heterogeneous catalysts: Structure and reactivity. J. Electron Spectrosc. Relat. Phenom. 1994, 68, 569-578.
- (50) VanGelder, L. E.; Matson, E. M. Heterometal functionalization yields improved energy density for charge carriers in nonaqueous redox flow batteries. *J. Mater. Chem. A* **2018**, *6*, 13874–13882.
- (51) Robin, M. B.; Day, P. Mixed Valence Chemistry: A Survey and Classification; New York, 1968; Vol. 10.
- (52) Sheldrick, G. M. SHELXT-2014/5. University of Götingen: Göttingen, Germany, 2014.
- (53) Sheldrick, G. Crystal structure refinement with SHELXL. Acta Crystallogr., Sect. C: Struct. Chem. 2015, 71, 3-8.
- (54) Barr, T. L.; Seal, S. Nature of the use of adventitious carbon as a binding energy standard. *J. Vac. Sci. Technol., A* 1995, *13*, 1239–1246.